

# High frequency limit for single-electron pumping operations

Chuan-Yu Lin<sup>1</sup> and Wei-Min Zhang<sup>1,\*</sup>

<sup>1</sup>*Department of Physics and Center for Quantum information Science,  
National Cheng Kung University, Tainan 70101, Taiwan*

(Dated: Dec. 2, 2010)

In this Letter, we study the transient electron transfer phenomena of single-electron devices with alternating external gate voltages. We obtain a high frequency limit for pumping electrons one at a time in single-electron devices. Also, we find that in general the electrical current is not proportional to the frequency of the external signals in the single-electron devices, due to the strong quantum coherence tunneling effect.

PACS numbers: 85.35.Gv, 73.63.-b, 03.65.Yz

Single-electron pumps and turnstiles are nanoscale tunneling devices utilizing controllable transfer of electrons one-by-one synchronized with alternating external gate voltages. These devices are supposed to have important applications as current standards and also as high-frequency amplifiers/detectors in solid-state quantum computing. Single-electron pumping operations have been experimentally demonstrated with various nanoscale tunneling structures [1–8]. However, most of experimental realizations for single-electron turnstiles are basically at the level of classical charge dynamics with relatively low signal frequencies ( $\sim$  tens to hundreds MHz) and the relatively small pumped current ( $\sim$  a few pA). To achieve the device as a quantized source of electron current, we shall closely monitor the electron transfer in single-electron devices in the high frequency region to find the optimal conditions for single-electron pumping operations.

Previous studies concerning electron transport in various nanodevices have largely been focusing on the understanding and prediction of the steady-state transport phenomena [9, 10]. Time-dependent nonequilibrium transport are much more complicated [11–13]. However, for a nanodevice, in particular, for quantum devices, the big challenge is to understand and predict not only how fast or slow a nanoscale device can turn on or off a current, but also how reliably and efficiently the device can maintain the quantum coherence through external field controls. Furthermore, it is also challenging to manipulate the quantum device by driving the contacts far away from equilibrium. These challenges require a full understanding of the time-dependent quantum transport intimately entangling with quantum coherence of electrons in the device. Therefore, in this Letter, we shall utilize the nonequilibrium quantum transport theory for nanodevices we developed recently [13] to monitor the real-time dynamics of electronic transfer in single-electron devices with high frequency external gate voltage, to understand the features of devices far away from equilibrium.

A typical single-electron device consists of three seri-

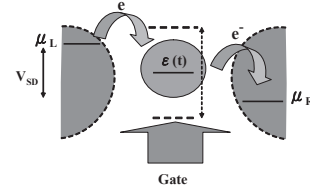


FIG. 1: A schematic plot of the single-electron turnstiles (a quantum dot device coupled to two leads), and Gate control the energy level of the dot in order to be the turnstile.

ally connected metallic islands and a gate coupled only to the central island. Here we model the central island as a quantum dot with a single energy level, as shown schematically by Fig. 1. The pump or turnstile operations are realized by imposing the repetitive pulses to the gate. When an alternating voltage is applied to the gate, electrons can be transferred one-by-one between the source and the drain during every voltage pulse under certain conditions. We will apply a harmonic time modulation to vary the energy level of the dot,  $\varepsilon(t) = \varepsilon_0 + \varepsilon_c \sin(\omega_c t)$ , and a dc bias voltage  $V_{SD}$  between the source and drain to examine the electron transfer dynamics.

Based on the recently developed non-equilibrium quantum transport theory for nanodevices [13], the electron occupation number in the dot and the transient electron current from the leads into the dot are given by

$$n(t) = v(t, t) + u(t, t_0)n(t_0)u^\dagger(t, t_0), \quad (1a)$$

$$I_{L,R}(t) = -\frac{2e}{\hbar} \text{Re} \int_{t_0}^t d\tau \text{Tr} \left\{ g_{L,R}(t, \tau) v(\tau, t) - \tilde{g}_{L,R}(t, \tau) \times u^\dagger(t, \tau) + g_{L,R}(t, \tau) u(\tau, t_0) n(t_0) u^\dagger(t, t_0) \right\}, \quad (1b)$$

respectively, where  $L, R$  denote the left and right leads (source and drain). The functions  $u(\tau, t_0)$  and  $v(\tau, t)$  in Eq. (1) are related to the retarded and correlation Green functions that satisfy the integrodifferential equations of

\*Electronic address: wzhang@mail.ncku.edu.tw

motion [13, 14]:

$$\dot{u}(\tau, t_0) + i\varepsilon(\tau)u(\tau, t_0) + \int_{t_0}^{\tau} d\tau' g(\tau, \tau')u(\tau', t_0) = 0, \quad (2a)$$

$$v(\tau, t) = \int_{t_0}^{\tau} d\tau' \int_{t_0}^{\tau'} d\tau'' u(\tau, \tau') \tilde{g}(\tau', \tau'') u^\dagger(t, \tau''), \quad (2b)$$

subjected to the initial condition  $u(t_0, t_0) = 1$ .  $n(t_0)$  in Eq. (1) is the initial electron occupation in the dot. Here, we have defined  $g(\tau, \tau') = \sum_{\alpha=L,R} g_\alpha(\tau, \tau')$  and  $\tilde{g}(\tau, \tau') = \sum_{\alpha=L,R} \tilde{g}_\alpha(\tau, \tau')$ .  $g_{L,R}(\tau, \tau')$  and  $\tilde{g}_{L,R}(\tau, \tau')$  are the time-correlation of electron transferring in the leads through the dot [14]:

$$g_{L,R}(\tau, \tau') = \int_{-\infty}^{\infty} \frac{d\omega}{2\pi} J_{L,R}(\omega) e^{-i\omega(\tau-\tau')}, \quad (3a)$$

$$\tilde{g}_{L,R}(\tau, \tau') = \int_{-\infty}^{\infty} \frac{d\omega}{2\pi} J_{L,R}(\omega) f_{L,R}(\omega) e^{-i\omega(\tau-\tau')}, \quad (3b)$$

in which  $f_{L,R}(\omega) = \frac{1}{e^{\beta(\omega-\mu_{L,R})} + 1}$  are the initial electron distribution functions in the leads at the initial temperature  $\beta = 1/k_B T$ , and  $\mu_{L,R}$  the corresponding chemical potentials.  $J_{L,R}(\omega) = 2\pi\rho_{L,R}(\omega)|V_{L,R}(\omega)|^2$  are the spectral densities with  $\rho_{L,R}(\omega)$  being the densities of states of the leads  $L$  and  $R$ , and  $V_{L,R}(\omega)$  the lead-dot coupling coefficients. In reality, most of spectral densities have more or less a Lorentzian-type shape,

$$J_{L,R}(\omega) = \frac{\Gamma_{L,R} d_{L,R}^2}{(\omega - \mu_{L,R})^2 + d_{L,R}^2}, \quad (4)$$

where  $\Gamma_{L,R}$  are the electron tunneling rate from the leads to the dot, and  $d_{L,R}$  are the bandwidths of the spectral densities. The integral kernels,  $g_{L,R}(\tau, \tau')$  and  $\tilde{g}_{L,R}(\tau, \tau')$ , characterize all the back action memory effects between the leads and dot associating with quantum dissipation and fluctuation. These effects must be fully taken into account for the accuracy of single-electron transfer.

The above transient quantum transport theory can reproduce the time-dependent transport theory of mesoscopic systems developed by Jauho *et al.* based on Keldysh's nonequilibrium Green function technique [11]. The main advantage of the present theory is that it takes into account explicitly the initial state dependence of the device [13]. Thus the time-dependent electron transfer in single-electron devices can be monitored with alternating external gate voltages from an arbitrary initial state of the device. In the following calculation, we take  $n(t_0) = 0$ . The detailed results are plotted in Figs. 2-5, where we take the tunneling rate  $\Gamma_L = \Gamma_R = \frac{1}{2}\Gamma$ . The applied bias voltage  $V_{SD}$  is set to be a constant, and the dot energy level varies with time:  $\varepsilon(t) = \varepsilon_0 + \varepsilon_c \sin(\omega_c t)$ , where the signal frequency will be set as a function of  $\Gamma$  to examine the validity of the high frequency operation for pumps and turnstiles. The initial temperature of the

leads is taken at  $k_B T = 0.1\Gamma$ . We also fix the bandwidth of the spectral density:  $d_{L,R} = 20\Gamma$  which is close to the wide band limit. All the parameters can be controlled experimentally. In the rest of the Letter, we will focus on the electron transfer phenomena of the device at different input parameters to understand the transient electron dynamics in the single-electron devices.

Fig. 2 plots the electron population in the dot, the left and right current flowing into the dot as well as the net current passing through the dot at the signal frequency  $\omega_c = 4\Gamma$  with different signal strength (amplitude)  $\varepsilon_c$ . The bias voltage  $eV_{SD} = 4\Gamma$  is added symmetrically to the source and drain while the energy level of the dot is set  $\varepsilon_0 = 2\Gamma$ . In Fig. 2(a), the dotted line is plotted for the time dependence of the signal (harmonic modulation) and the solid line is for the electron population in the dot. The result shows that the electron population in the dot oscillates between 0.3 ~ 0.7 with the same frequency as that of the signal, except for a phase shift. The electron population does not vary between zero to one is due to the quantum coherent tunneling of the electron between the leads and the dot. The currents are plotted in Fig. 2(b). The results show that the currents  $I_L(t)$  and  $I_R(t)$  oscillate with the same signal frequency but the oscillating shapes are deformed slightly from the sinusoid with a rather small phase shift. The net current  $I(t)$  which depicts the electron transfer from the left to right leads shows to be a perfect sinusoidal oscillation, with the oscillating frequency being the twice of the signal frequency, as a result of symmetrically applying the harmonic modulation to the dot with respect to the source and drain. In Fig. 2(c) we plot the time dependence of the electron population at different signal strengths. As one can see, increasing the signal amplitude  $\varepsilon_c$  enhances the oscillating amplitude of the electron population. It is interesting to find that when  $\varepsilon_c \simeq 6\Gamma$ , the oscillating amplitude of the electron population reaches the maximal value. Continuously increasing the signal strength will weaken the population oscillations. The same situation happens for the current, the current oscillation amplitude reaches the maximal value at  $\varepsilon_c \simeq 6\Gamma$ . Further increasing the signal strength will decrease the strength of the current oscillation.

Next, we shall vary the signal frequency to see the corresponding change of the transfer phenomena. Fig. 3 plots the same physical quantities at the signal frequency  $\omega_c = 2\Gamma$ . The electron population in the dot behaves almost the same, see Fig. 3(a). The left and right currents  $I_L(t)$  and  $I_R(t)$  still oscillate with the signal frequency but a photon-assisted peak appears as a nonlinear response to the signal. The net current  $I(t)$  remains in a good oscillating profile with the oscillating frequency still being the twice of the signal frequency, as shown in Fig. 3(b). Fig. 3(c)-(d) plot the electron population and the net current with different signal strengths. Again, we find that the signal strength for maximal amplifying locates at  $\varepsilon_c \simeq 6\Gamma$  where both the electron population and current oscillate with maximal amplitudes. Contin-

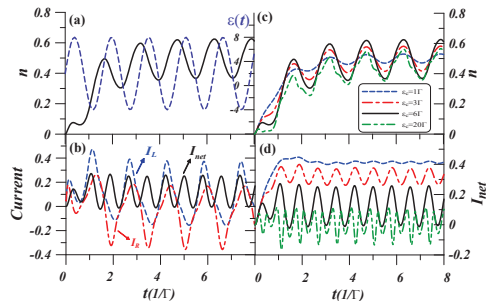


FIG. 2: The time-dependent electron transfer phenomena in the single-electron turnstile. (a) The Harmonic time modulation (the dotted line):  $\varepsilon(t) = \varepsilon_0 + \varepsilon_c \sin(\omega_c t)$  with  $\varepsilon_0 = 2\Gamma$ ,  $\varepsilon_c = 6\Gamma$  and  $\omega_c = 4\Gamma$ , and the electron population (the solid line) in the dot; (b) the corresponding electron transfer currents  $I_L(t)$ ,  $I_R(t)$  and  $I_{\text{net}}(t)$ ; (c) and (d) are the electron population and the net current with different signal strength  $\varepsilon_c$ , respectively.

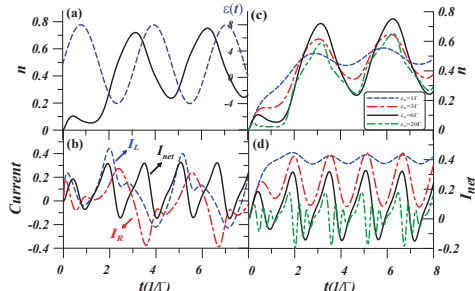


FIG. 3: The same plots as in Fig. 2 with a different signal frequency  $\omega_c = 2\Gamma$ .

ously increasing the signal strength only induces more photon-assisted peaks but does not amplify the transfer current, where the photon-assisted peaks occur near  $\varepsilon = \varepsilon_0 \pm 2k\omega_c$  and  $k$  is an integer.

To further analyze the controllable electron transfer in the device, we vary the dc bias voltage  $V_{\text{SD}}$  applied to the leads. Fig. 4 plots the electron population and the net current with different bias. In Fig. (4(a)-(b)), the bias  $eV_{\text{SD}} = 6\Gamma$  is symmetrically applied to the leads with  $\varepsilon_0 = 3\Gamma$ , while in Fig. (4(c)-(d)), the bias  $eV_{\text{SD}} = 5\Gamma$  is asymmetrically applied to the leads with  $\varepsilon_0 = 2\Gamma$ . As we see the electron population and the net current do not show a qualitative difference in both cases. However, the asymmetric case do change the profile of the net current due to the breaking of the symmetry.

Comparison with the results in Figs. 2-4, we find that amplifying the electron transfer in the single-electron devices is mainly controlled by the signal frequency and the signal strength. The signal strength  $\varepsilon_c \simeq 6\Gamma$  is an optimal operation condition for the single-electron device reaching the maximal amplifying. In Fig. 5, we plot the maximal oscillating amplitudes of the electron population and the net current varying with different signal frequency  $\omega_c$  at  $\varepsilon_c = 6\Gamma$ . As we see the oscillating ampli-

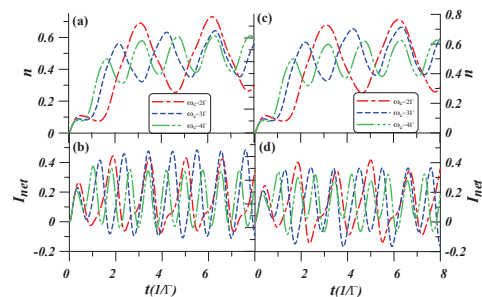


FIG. 4: Electron population and the net current for different bias voltages. (a)-(b) The bias  $eV_{\text{SD}} = 6\Gamma$  is symmetrically applied to the leads with  $\varepsilon_0 = 3\Gamma$ . (c)-(d) The bias  $eV_{\text{SD}} = 5\Gamma$  is asymmetrically applied to the leads with  $\varepsilon_0 = 2\Gamma$ . Here  $\varepsilon_c = 6\Gamma$

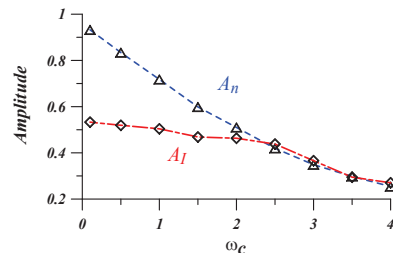


FIG. 5: The oscillation amplitudes of the electron population in the dot (given by  $A_n$ ) and the current flowing from the left to right leads (given by  $A_I$ ) with varying the signal frequency  $\omega_c$ . Here  $eV_{\text{SD}} = 4\Gamma$ ,  $\varepsilon_0 = 2\Gamma$  and  $\varepsilon_c = 6\Gamma$ .

tude of electron population increases with the decreasing of the signal frequency  $\omega_c$ . It will approach to almost one with a relative low frequency ( $\omega_c < 0.1\Gamma$ ). This provides a high signal frequency limit (in terms of tunneling rate  $\Gamma$ ) for the single electron device acting as a single-electron pump. With higher frequencies, can an electron only be partially occupied in the dot, due to the strong quantum coherence of electrons between the leads and dot. In other words, the electron occupation number in the dot can never be perfectly one or zero in the high frequency region ( $\sim \Gamma$ ). The oscillating amplitude of the net current also increases with decreasing the signal frequency  $\omega_c$  but when  $\omega_c < 2\Gamma$ , the oscillating amplitude of the net current approaches to a constant, as shown in Fig. 5. This indicates that the electrical current is not proportional to the frequency of the external signals. Taking the experimental value  $\Gamma = 50\mu\text{eV}$  in [4], the high frequency limit for single-electron pumps is  $\omega_c \simeq 7.5\text{MHz}$ . For the experimental data  $\Gamma = 50\text{meV}$  [5], single-electron pumps works for the signal frequency  $\omega_c < 0.1\Gamma \simeq 7.5\text{GHz}$ . These solutions are consistent with the current experimental results [4, 5].

In conclusion, the above analysis and discussion show a general picture how the electron population in the dot and the current passing through the dot response to the frequency and the strength of the alternating external gate voltage. With a harmonic time modulation, we find

that the optimal operations for the single electron device is near the signal strength  $\varepsilon_c \simeq 6\Gamma$ . Due to the strong coherence tunneling at high frequency regime, the single-electron pumps or turnstiles works only at the signal frequency  $\omega_c < 0.1\Gamma$ . Realistic single-electron devices involve much more complicated nanostructures [1–8] than the simplified model considered in the present work, but our rigorous analysis could provide a useful guide for high

frequency operations of single-electron pumps and turnstiles. On the other hand, the strong quantum coherence of the electron transfer in high frequency region shows that single-electron device operations at high frequency are promising for quantum information processing [15].

This work is supported by the National Science Council of ROC under Contract No. NSC-99-2112-M-006-008-MY3 and National Center for Theoretical Science.

- 
- [1] L. J. Geerligs, V. F. Anderegg, P. A. M. Holweg, J. E. Mooij, H. Pothier, D. Esteve, C. Urbina, and M. H. Devoret, *Phys. Rev. Lett.* **64**, 2691 (1990).
- [2] M. W. Keller, A. L. Eichenberger, J. M. Martinis, and N. M. Zimmerman, *Science* **285**, 1706 (1999).
- [3] S. V. Lotkhov, S. A. Bogoslovsky, A. B. Zorin, and J. Niemeyer, *Appl. Phys. Lett.* **78**, 946 (2001).
- [4] A. Fujiwara, N. M. Zimmerman, Y. Ono, and Y. Takahashi, *Appl. Phys. Lett.* **84**, 1323 (2004); A. Fujiwara, K. Nishiguchi and Y. Ono, *Appl. Phys. Lett.* **92** 042102 (2008).
- [5] M. D. Blumenthal, B. Kaestner, L. Li, S. Giblin, T. J. B. M. Janssen, M. Pepper, D. Anderson, G. Jones and D. A. Ritchie, *Nat. Phys.* **3**, 343 (2007).
- [6] J. P. Pekola, J. J. Vartiainen, M. Möttönen, O.-P. Saira, M. Meschke, and D. V. Averin, *Nat. Phys.* **4**, 120 (2008).
- [7] A. Kemppinen, S. Kafanov, Yu A. Pashkin, J. S. Tsai, D. V. Averin and J. P. Pekola, *Appl. Phys. Lett.* **94** 172108 (2009).
- [8] S. P. Giblin, S. J. Wright, J. D. Fletcher, M. Kataoka, M. Pepper, T. J. B. M. Janssen, D. A. Ritchie, C. A. Nicoll, D. Anderson, and G. A. C. Jones, *New J. Phys.* **12**, 073013 (2010).
- [9] S. Datta, *Electronic Transport in Mesoscopic Systems*, (Cambridge, England, 1995).
- [10] H. Haug and A. P. Jauho, *Quantum Kinetics in Transport and Optics of Semiconductors*, Springer Series in Solid-State Sciences 123, 2nd Ed. (Springer-Verlag, Berlin, 2008).
- [11] A.-P. Jauho, N. S. Wingreen, and Y. Meir, *Phys. Rev. B* **50**, 5528 (1994).
- [12] J. Maciejko, J. Wang, and H. Guo, *Phys. Rev. B* **74**, 085324 (2006).
- [13] J. S. Jin, M. W. Y. Tu, W. M. Zhang, Y. J. Yan, *New J. Phys.* **12**, 083013 (2010).
- [14] M. W. Y. Tu and W. M. Zhang, *Phys. Rev. B* **78**, 235311 (2008).
- [15] G. Feve, A. Mahe, J.-M. Berroir, T. Kontos, B. Placais, D. C. Glattli, A. Cavanna, B. Etienne and Y. Jin, *Science* **316**, 1169 (2007).